IV International Conference on Particle-based Methods – Fundamentals and Applications
PARTICLES 2015
E. Oñate, M. Bischoff, D.R.J. Owen, P. Wriggers & T. Zohdi (Eds)

AN APPLICATION OF THE FINITE-DISCRETE ELEMENT METHOD IN THE SIMULATION OF CERAMIC BREAKAGE: METHODOLOGY FOR A VALIDATION STUDY FOR ALUMINA SPECIMENS

A. FARSI[1], J. XIANG[1], J. P. LATHAM[1], A. D. PULLEN[1†], M. CARLSSON[2], E. H. STITT[2], M. MARIGO[2]

[1]Applied Modelling and Computation Group (AMCG),
Department of Earth Science and Engineering
[1†]Department of Civil and Environmental Engineering
Imperial College London, South Kensington Campus,
London SW7 2AZ, United Kingdom

[2]Johnson Matthey, P.O. Box 1, Belasis Avenue,
Billingham, Cleveland, TS23 1LB, United Kingdom

Key words: Ceramics, Fracture, FEMDEM, Multi-body systems

Abstract. Alumina (aluminum oxide, Al_2O_3) particles are pelletised and fired to produce high porosity catalyst pellets of complex shapes. These pellets fill cylindrical reactor columns with particulate packing structures that are key to the in-service performance, but will suffer breakages which impact on catalyst performance. The combined Finite-Discrete Element Method (FEMDEM) is ideally suited to the simulation of both the multi-body pellet dynamic packing and quasi-static interactions as well as the stress field of each individual pellet, its deformations and fragmentation. The application of FEMDEM fracture modelling to a fine-grained brittle and porous material is novel. This paper presents a methodology for a validation study through comparison with three point-bending and Brazilian tests and discusses FEMDEM's potential in modelling multi-body fragile systems.

1 INTRODUCTION

The combined Finite-Discrete Element Method (FEMDEM) [1] has been widely employed in computational modelling in the last decade, mostly for geomechanical applications. Recently some validation studies have been carried out for both rock fragmentation [2] and multi-body interactions [3]. The application of FEMDEM simulations to describe the behaviour of porous ceramics is novel and its employability needs to be assessed. The methodology for a validation study is now presented. The specimens selected for the validation work are fired at three different temperatures to obtain the three grades of porosity

in the range 0.15-0.36. Their associated properties are characterised by Vickers indentations, and three-point bending tests for the purpose of model calibration. The specimens are also analysed by Field Emission Scanning Electron Microscopy (FESEM) to investigate the type of porosity and the pore size distribution within the sample cross sections to evaluate the homogeneity of their microstructure. Laboratory test load-displacement curves and high-speed video images are compared to the numerical results obtained from FEMDEM. Digital image correlation and tracking methods are employed to compare the fracture path and the displacement of the fragments during the experiment with the numerical results. The numerical model describes the entire experimental apparatus as a multi-body problem with the cross-head impacting on the specimen. This enables more realistic modelling of the effects of compliant rig components where the sample interacts with the lower constraint supports and the axial driving punch above and therefore of the actual forces and displacements during the experiment. The code is fully dynamic and can represent dynamic effects such as strain waves propagating through the specimens and the testing apparatus. This paper presents the intriguing post-failure behaviour as observed in the experiments and as captured by the simulation and discusses the potential for this methodology to model multi-body fragile systems.

2 SAMPLES

Prismatic and cylindrical specimens have been selected for the validation work. All the specimens are sintered with a reference alpha-alumina powder, which is compacted at an initial porosity of 0.45 and then fired at 1200°C, 1300°C and 1400°C respectively to obtain three sets of bars and pellets with final porosity of 0.36, 0.26 and 0.15. The 0.36 porosity specimens are shown in Figure 1. Porosimetry and densitometry tests are employed to assess the pore size distribution and density of the specimens for the different firing temperatures. The specimens are also analysed by field emission scanning electron microscope to investigate the type of porosity and the pore size distribution within the sample cross sections to evaluate the homogeneity of their microstructure. The porosity of the ceramic specimens does not present important variations along the cross section, allowing them to be considered homogeneous and isotropic. The specimens of each set are then tested with Vickers indentations and three-point bending tests to infer the Young's modulus and tensile strength. The mechanical properties are then compared with the values for porous alumina ceramics found in literature [4] and [5] and the energy release rate is calculated on the basis of correlation curves presented in literature.

3 THREE-POINT BENDING AND BRAZILIAN TESTS

Two different experiments have been selected for the validation work on ceramic breakage. The three-point bending test consists of placing a specimen on two supports and applying a vertical load in the middle of the two supports by means of a punch. Before failure, according to the Euler-Bernoulli beam theory, a homogeneous bar experiences the

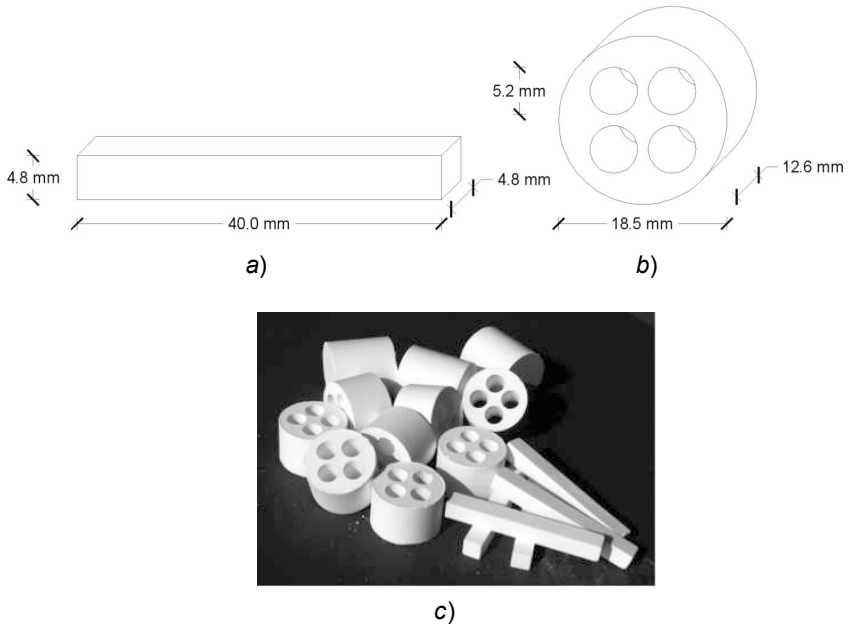

Figure 1: Final geometry of the 0.36 porosity a) bars and b) cylinders with holes. c) Photograph of the tested materials.

maximum tensile and compressive stress respectively in its bottom and top surfaces, in the exact middle of the two supports. Since the tested material fails under tensile stress before it fails under compression, a fracture will initiate from the bottom side when the tensile stress reaches the value of the tensile strength of the tested material. By solving the Euler-Bernoulli differential equation it is possible to express the maximum tensile stress experienced by the specimen as a function of the applied load and moreover infer the tensile strength (f_t) and the Young's modulus (E) from the maximum force (F) and deflection (w) applied to the beam before failure.

$$f_t = \frac{3Fs}{2H^3} \tag{1}$$

$$E = \frac{Fs^3}{4wH^4} \tag{2}$$

In equations (1) and (2) s is the span between the two supports and H is the height and width of a bar with a square cross-section. As mentioned before, the stress field induced in the specimen by the controlled boundary conditions not only restricts the area where the fracture can initiate, but also constrains the opening mode when the fracture is propagating. In fact, neglecting the possible effects of microscale inhomogeneities and anisotropies, the material points that are failing experience a pure horizontal extension,

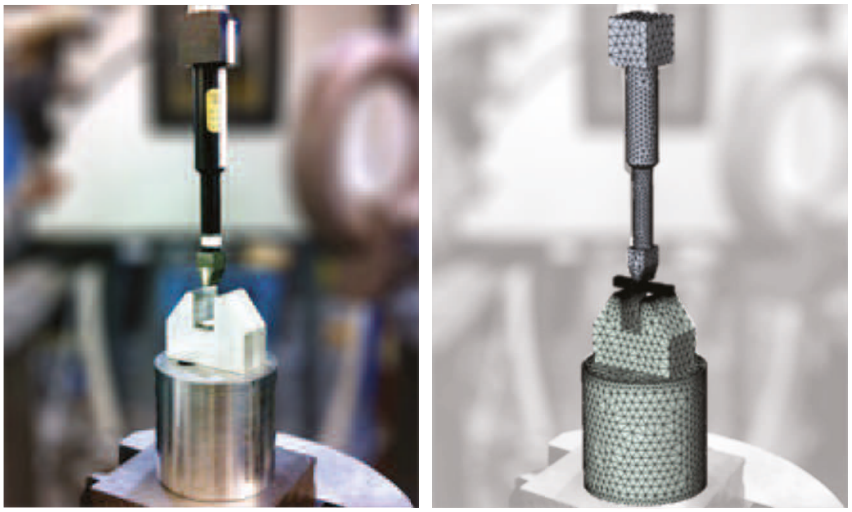

Figure 2: a) Photograph of the real three-point flexural test apparatus and b) tetrahedral mesh in its 3D numerical simulation.

which is normal to the plane of the crack, in a mode I opening fashion. The apparatus in Figure 2 is the one used in the experiments. A metal support with a 20 mm span is fixed to a steel cylinder. The punch is a steel cross-head instrumented with a load cell and attached to an actuator. The experiment is executed in displacement control, with a cross-head velocity of 0.5 mm/min.

The three-point bending apparatus is mounted on actuators of different size, depending on the velocity of the test. The testing machine can record forces and displacements during the experiment. A second data logger is connected to the force transducer that has been fixed on the cross-head. This makes it possible to record the force at a higher frequency and to have a more consistent set of measurements, for example when the experiment is performed with different actuators. The experiment is also recorded with a high-speed camera, which enables the correction of errors in the force-deflection curve resulting from possible rig compliances and localised plastic deformation at the points of contact. The deflection is set to zero where the linear extension of the curve intersects the horizontal axis. The corrected deflection of the beam before failure is then calculated by subtracting the average of the two displacements in the points of contact with the supports from the displacement of the midpoint as illustrated in Figure 3. The high-speed video is also employed to determine the fracture path and velocity of the fragments.

The experiment is modelled with 2D and 3D FEMDEM simulations. The boundary conditions and the 2D triangular mesh are illustrated in Figure 4. The top of the punch is constrained with constant velocity. To reduce the run time of the numerical simulation, the velocity of the constraint is set to 0.1 m/s. Although this loading rate is significantly higher than the one in the laboratory experiment, it induces a quasi-static response in

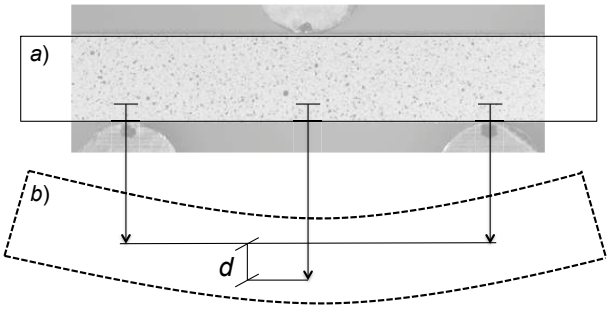

Figure 3: a) Beam before contact with no deformation and b) immediately before failure with deflection d calculated as the difference between the displacement of the midpoint and the average of the two displacements of the points of contact with the supports.

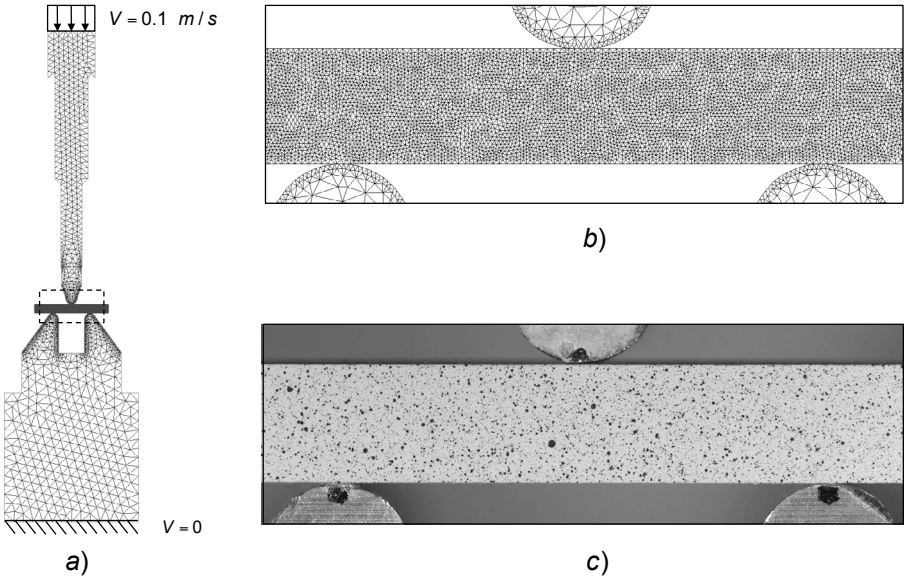

Figure 4: a) Boundary conditions for the three-point flexural experiment and triangular mesh of its 2D numerical simulation. b) Detail of the specimen discretisation and c) corresponding frame from the high-speed video.

the bar as there is no significant difference between the force applied by the punch and the one applied by the two constraints. To further reduce the calculation time, when the simulation starts, the punch is in contact with the specimen and for this reason an initial velocity equal to the one applied to the constraint is imposed to the whole punch. The discretisation of the punch and constraints is refined only where the contact occurs so as to better represent the geometry of their contours without considerably increasing the computational burden. The specimen is discretised with an unstructured fine mesh to correctly represent both the de-bonding stress during the opening of the crack and the fracture path along the element boundaries. The total number of elements employed in the model is around 20,000. The material properties used to describe the three-point bending apparatus are E_s=210 GPa, ν_s=0.3 and ρ_s=7850 kg/m^2, where E_s is the Young's modulus, ν_s is the Poisson's ratio and ρ_s is the density. The material properties used for the specimens vary depending on the porosity of the tested sample: the reported results refer to the 0.36 porosity set with E_c=60 GPa, ν_c=0.22, ρ_c=2560 kg/m^2 and f_t=78 MPa. The interaction between the steel and the alumina sample is modelled using a Coulomb coefficient of friction equal to 0.01.

$$\sigma_h = \frac{6EH}{s^2} w \tag{3}$$

The mean and horizontal stress fields in the apparatus and in the tested specimen respectively at different time lapses are reported in Figure 5. The simulated stress field in the bar sample before failure agrees with the theoretical predictions of Euler-Bernoulli beam theory. Equation (3) represents the relation between beam deflection and the horizontal stresses experienced by the material point between the two supports in the bottom side of the beam before failure. In Figure 6*a* this analytical solution is compared with the horizontal stress calculated in the corresponding FEMDEM simulation. In accordance with the analytical solution, the horizontal stress extrapolated from the simulation increases linearly until it reaches the value of the tensile strength (78 MPa) and then, when the fracture starts to propagate, it drops to zero. The numerical model slightly overestimates the displacements (and thus underestimate the stiffness) due to the joint element discretisation [6]: this leads to a slightly lower gradient for the numerical curve. In Figure 6*b* the force-deflection curve calculated in the numerical simulation is compared with three experimental results. The maximum value for the contact force is slightly higher in the numerical results than in the theoretical prediction: this can be because the mesh elements are not all perfectly aligned across the vertical plane where the stress field develops its maximum tension. The fracture path produced in the numerical simulations is close to the one observed in the experiments as shown in Figure 5*b*.

The second experiment used to validate the simulation is a Brazilian disc test on alumina catalyst supports. The test consists of placing a cylindrical pellet between two plates and diametrically compressing it to failure. This type of experiment is often used as an indirect

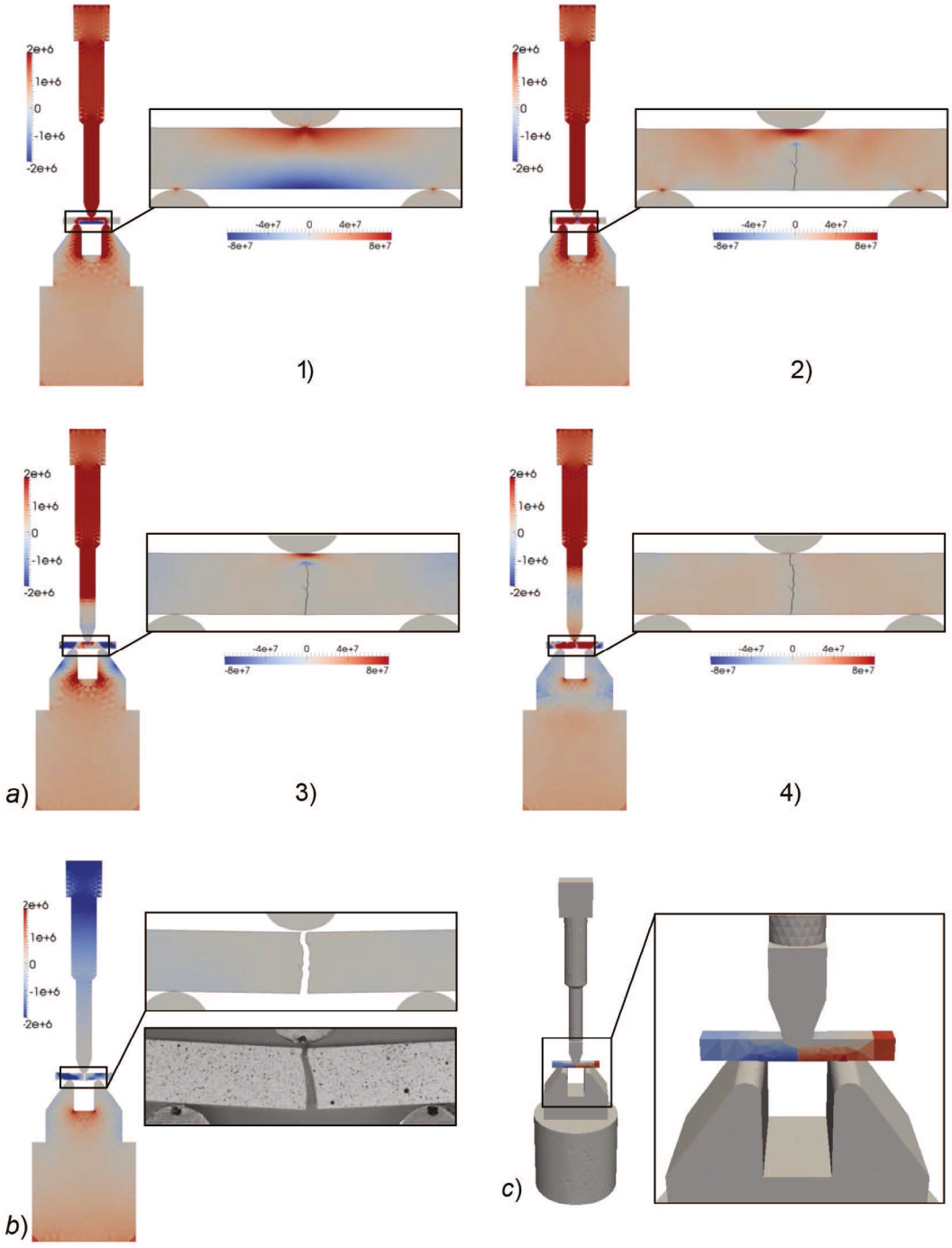

Figure 5: a) Stress field in a 2D numerical model showing a crack propagating at different times during a three-point flexural test: the mean stress for each time lapse is shown on the image of the apparatus on the left and the horizontal stress is shown on the magnified beam on the right. b) Comparison between the model of the specimen after failure in the 2D numerical simulation and a frame from the high-speed video recording of the actual experiment. c) Horizontal displacement field in a 3D numerical model.

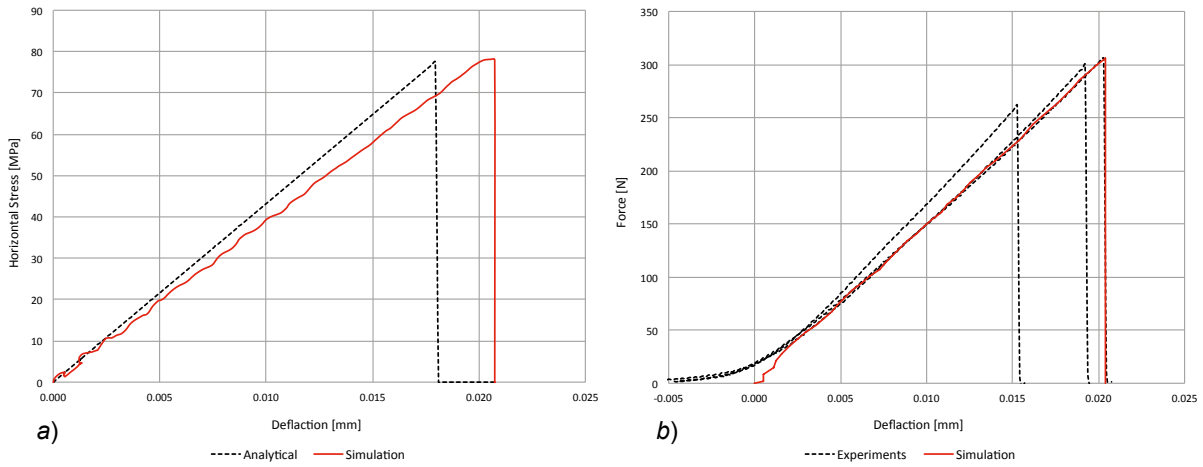

Figure 6: a) Comparison of the vertical displacement and the horizontal stress experienced by the material point between the two supports in the bottom side of the beam in a 2D numerical model and in the analytical solution. b) Force-deflection curves calculated in the numerical simulation and obtained from three experiments.

testing method to evaluate the tensile strength of brittle materials such as concrete, rock, and ceramics. The compression induces a stress field with horizontal tensile stress which according to a linear elastic model has its highest value in the centre of the disc. The tensile strength can be calculated based on the two-dimensional elastic solution for a disc with two concentrated forces applied to its vertical extremes. It is then possible to express the horizontal tensile stress experienced by the specimen in the centre of the disc as a function of the applied load (F) and of the geometry of the sample.

$$f_t = \frac{2F}{\pi D t} \tag{4}$$

Assuming that failure occurs at the point of maximum tensile stress, i.e. at the centre of the disc, the Brazilian test formula (4) gives an estimate of the indirect tensile strength (f_t), where D is the diameter of the disc and t its width [7]. Similarly to the three-point bending experiment, the first material point that is failing experiences a horizontal extension, normal to the plane of the crack, in a mode I opening fashion. However, this equation does not take into account defects, local crushing and plastic deformations at the points of contact, which might affect the stress field induced in the cylinder. The presence of holes in the disc, such as in a catalyst support, has the effect of generating a more complex stress field that cannot be precisely described by the equation above. At failure, the opening mode can also be affected, producing a shear crack. A FEMDEM simulation is capable not only of representing the stresses and deformations of a disc with holes before failure, but also of replicating the fracture propagation in a mixed mode

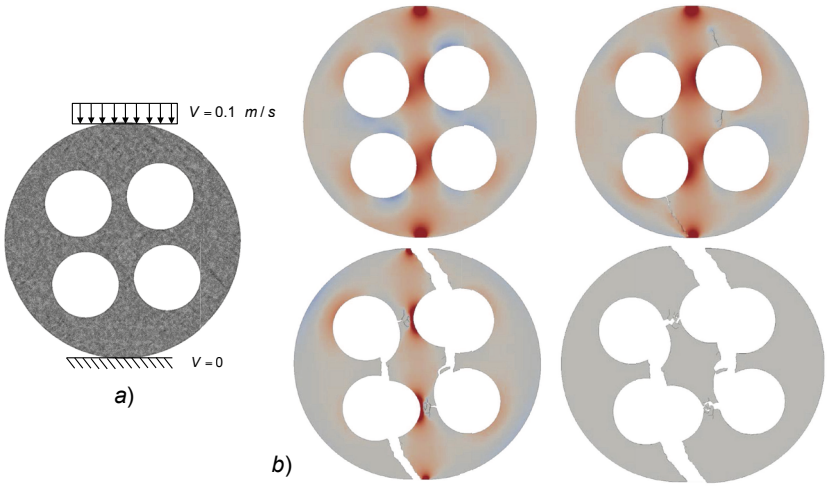

Figure 7: a) Boundary conditions for the Brazilian test of a ceramic pellet with four holes diametrically compressed against two steel plate and triangular mesh of its 2D numerical simulation. b) Time-lapse numerical results immediately before failure and after failure.

opening fashion, as shown in Figure 7*b*, where the test is modelled with a 2D simulation. The boundary conditions and the triangular mesh are shown in Figure 7*a*. The top plate is constrained with a constant vertical velocity of 0.1 m/s. Similarly to the three-point bending model, the specimen is discretised with an unstructured fine mesh to correctly represent both the de-bonding stress during the opening of the crack and the fracture path along the boundaries of elements. The total number of elements employed in the model is around 70,000. The methodology proposed for this validation work consists of repeating the test for different orientations of the axes of symmetry defined by the hole positions and for each of the three porosity sets and then comparing the force displacement curves, fracture paths and fragment sizes against the numerical results. More precisely, the pellets are compressed not only in their weak and strong orientations, but also in the other mixed configurations: the numerical results for the 0.36 porosity set are shown in Figure 8*a*.

4 MULTI-BODY CERAMIC SYSTEMS

Numerical analyses similar to those presented above can be applied to any type of pellet geometry and results can be employed for the evaluation of its mechanical performance. An example could be the shape and porosity analysis for the evaluation of the performance of catalyst supports, i.e. the ceramic pellets where the actual catalytic metal is dispersed, employed in fixed bed reactors. On the one hand a support needs to be highly porous to maximise the total surface area and therefore its catalytic activity, but on the other a high porosity can make the support too weak and unsuitable for the loading and operating conditions (Figure 8*b*). Also, during the standard lifecycle of the plant some of the ceramic pellets are crushed to fragments due to the thermal contractions of the reactors, reducing their service life and their efficiency. In particular, the accumulation of fine frag-

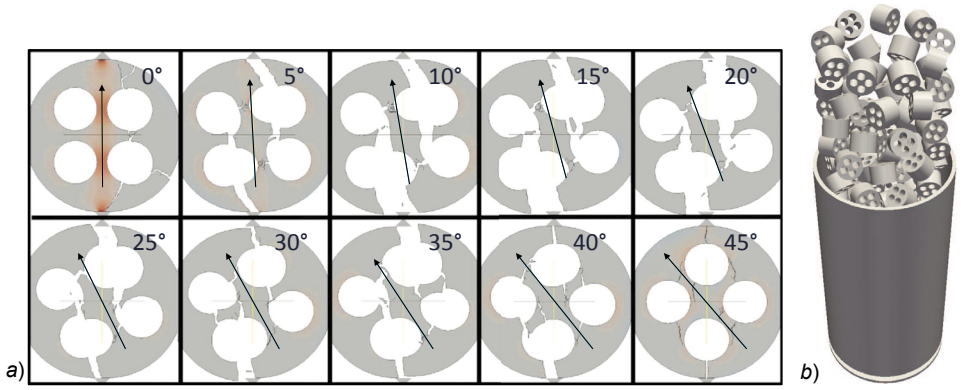

Figure 8: a) Pellet fragmentation during compression in different orientations and b) numerical simulation of the loading of alumina cylindrical pellets in a steel tube.

ments may produce localised reductions of permeability in the reactor, causing pressure drops and potentially reducing the lifetime of the reactor itself. FEMDEM simulations can be employed for the evaluation of the mechanical performance of catalysts to improve their strength, reduce the number of fine fragments at failure while meeting the required geometric surface area. Ultimately more realistic loading conditions, such as the compression applied by neighbouring catalysts due to the thermal shrinkage of the reactor, can be modelled for an even more precise evaluation of mechanical performances. To do this the operating conditions need to be replicated by modelling the packed structure of the fixed bed reactor. The problem of simulating the packing of cylindrical pellets in a tube has been approached with various computational techniques illustrated in literature. In [8] the packing process is simulated with both a semi-stochastic approach, where the particle path is randomly determined on the base of the overlapping of voxels, and a deterministic approach, where the repulsive forces and torques applied to the particles are calculated by measuring the number of their overlapping voxels and their voxel-level contact forces. In [9] these voxel-based methods are compared to discrete element simulations where the contact forces are calculated between pairs of spheres and the pellets are represented with clusters of spheres clumped together. A 3D FEMDEM simulation can be employed to simulate the pellets being cast into a reactor: pellets of any complex shape can be represented with a tetrahedral mesh and their contact forces are calculated with a penalty method and a Coulomb model of friction. An example is shown in Figure 9. A tube of 100 mm in diameter is filled with 220 ceramic pellets. Each particle is a cylinder of 18.5 mm diameter and 12.6 mm in width with 4 holes. As shown in Figure 9*a*, each pellet is discretised with 784 tetrahedra. The container is meshed with around 64,000 tetrahedra for a total of approximately 240,000 elements for the whole model. The geometries of the container and pellets have been imported from CAD drawings. All the particles are introduced in the domain above the container with a random orientation and a zero initial velocity. This process is completely automated through a pre-processing tool (POSITIT) that facilitates the control of filling conditions and avoids the need for a manually defined

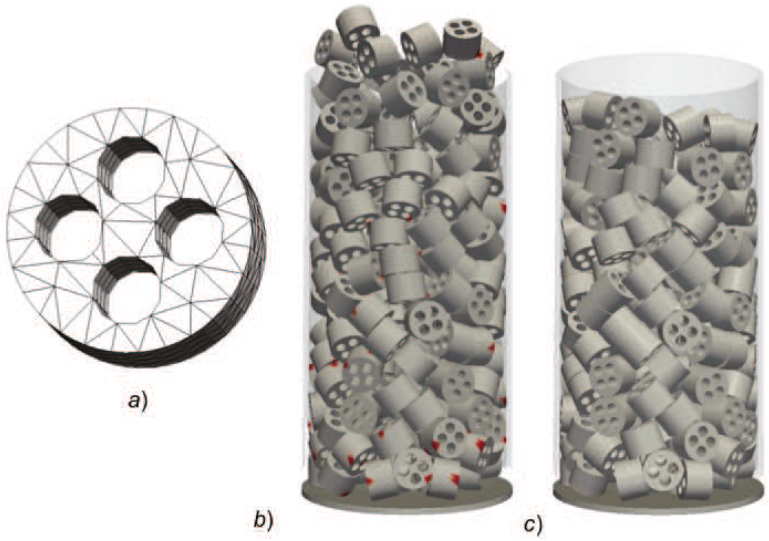

Figure 9: a) Tetrahedral mesh of a ceramic pellet with 4 holes, b) numerical results of pellet settlement simulation within a cylindrical container, with contact forces represented in red, and c) final packed structure after the filling process.

3D space for the initial conditions of each single pellet. In the numerical simulation in Figure 9*b* the pellets are modelled as rigid bodies with a density ρ_c=2560 kg/m^2 and the interaction between them is computed employing a Coulomb coefficient of friction equal to 0.4. Both the forces transmitted between the pellets and their points of contact can be extracted and visualised for each time step. The simulation runs in parallel on 10 cores in less then 24 hours. Alternatively, the same model can also be run in parallel employing deformable bodies to simulate not only the contact forces transmitted between the catalysts but also the stresses inside each particle.

5 CONCLUSIONS

Codes based on the combined Finite-Discrete Element Method (FEMDEM) are now widely applied in research: for industry applications more validation work needs to be done to demonstrate their robustness and accuracy in simulating complex dynamic fracture processes, especially in the context of porous ceramics. A novel methodology for the verification and validation of FEMDEM simulations has been the object of this paper. Some of the advantages of FEMDEM in modelling complex fragmentations by diametrical compression and multi-body interactions for ceramic materials have been presented. These include the explicit representation of fractures during the fragmentation process and the potential to represent complex-shaped bodies. Experimental and numerical results have been compared, confirming that a FEMDEM numerical simulation of mode I fracture in ceramic bars matches the experimental results of a three-point bending test. These results give a first confirmation that a FEMDEM code can be used for the evalua-

tion of catalyst mechanical performance. More confirmation can be obtained in the near future both by comparing the results obtained above for a Brazilian test simulation with the results from actual experiments and by employing the data extrapolated from more complex multi-body simulations of the packed structure inside the reactor.

ACKNOWLEDGEMENTS

The authors would like to thank Dogan Ozkaya for providing us with data from FESEM analysis and Daniel Curry for his help with sample preparation. This research is sponsored by EPSRC and the Johnson Matthey Technology Centre.

REFERENCES

[1] A. Munjiza, *The Combined Finite-Discrete Element Method*. Wiley, 2004.

[2] E. Rougier, E. Knight, S. Broome, a.J. Sussman, and a. Munjiza, "Validation of a three-dimensional Finite-Discrete Element Method using experimental results of the Split Hopkinson Pressure Bar test," *International Journal of Rock Mechanics and Mining Sciences*, vol. 70, pp. 101–108, Sept. 2014.

[3] J. Xiang, A. Munjiza, J.-P. Latham, and R. Guises, "On the validation of DEM and FEM/DEM models in 2D and 3D," *Engineering Computations*, vol. 26, no. 6, pp. 673–687, 2009.

[4] D. Lam, F. Lange, and A. Evans, "Mechanical properties of partially dense alumina produced from powder compacts," *Journal of the American Ceramic Society*, vol. 77, no. 8, pp. 2113–2117, 1994.

[5] J. Magdeski, "The porosity dependence of mechanical properties of sintered alumina," *Journal of the University of Chemical Technology and Metallurgy*, vol. 45, no. 2, pp. 143–148, 2010.

[6] E. Lorentz, "A mixed interface finite element for cohesive zone models," *Computer Methods in Applied Mechanics and Engineering*, vol. 198, no. 2, pp. 302–317, 2008.

[7] International Society for Rock Mechanics, "Suggested Methods For Determining Tensile Strength of Rock Materials," in *International Society for Rock Mechanics Commission on Standardization of Laboratory and Field Tests*, vol. 15, pp. 99–103, 1978.

[8] R. Caulkin, X. Jia, and C. Xu, "Simulations of structures in packed columns and validation by X-ray tomography," *Industrial & Engineering Chemistry Research*, pp. 202–213, 2008.

[9] R. Caulkin, W. Tian, M. Pasha, A. Hassanpour, and X. Jia, "Impact of shape representation schemes used in discrete element modelling of particle packing," *Computers and Chemical Engineering*, vol. 76, pp. 160–169, 2015.